

Il Mulinello

Georgia Institute of Technology

37th Annual VFS Student Design Competition



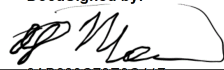
*Alex Moushegian
Milad Mozayyani
Alex Markov
Carlota Bonnet*



Il Mulinello

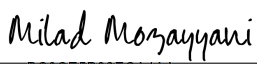
School of Aerospace Engineering
Georgia Institute of Technology
Atlanta, GA, 30332


37th Annual Vertical Flight Society Student Design Competition
Graduate Category
AE 8804 – Special Topics

DocuSigned by:

3AB680C79E9C417...
Alex Moushegian – Graduate Student
(Team Leader)
amoushegian3@gatech.edu

DocuSigned by:

2F69375727A94AB...
Alex Markov – Graduate Student
markov@gatech.edu

DocuSigned by:

BC0CE5B98ECA4AA...
Milad Mozayyani – Graduate Student
mmozayyani@gatech.edu

DocuSigned by:

E1BED3C220924D1...
Carlota Bonnet – Graduate Student
carlotabonnet@gatech.edu

DocuSigned by:

29518391F266425...
Dr. Marilyn J Smith – Faculty Advisor
marilyn.smith@ae.gatech.edu

DocuSigned by:

24CB8B4D9D8C4DE...
Dr. Dimitri Mavris – Faculty Advisor
dimitri.mavris@aerospace.gatech.edu

Acknowledgements

The *Il Mulinello* design team would like to thank those who helped us in this project.

Professors:

Dr. Marilyn J. Smith - Professor, Director of the Vertical Lift Research Center of Excellence, Daniel Guggenheim School of Aerospace Engineering, Georgia Institute of Technology

Dr. Dimitri Mavris - Regents Professor, Boeing Professor of Advanced Aerospace Systems Analysis, S.P. Langley Distinguished Professor, Director of the Aerospace Systems Design Laboratory, School of Aerospace Engineering, Georgia Institute of Technology

Dr. Jonnalagadda V R Prasad - Professor, Daniel Guggenheim School of Aerospace Engineering, Georgia Institute of Technology

Fellow Students:

A special thanks goes to Sara Pierson for her help with the control system

Thank you to Bob Walters, Lee Whitcher, Zujia Huang

COVID-19 Disclaimer

The impact of the COVID-19 pandemic on this project was primarily the cancellation of small-scale testing of airscrew geometries. The experimental test-rig was in the late stages of manufacturing with Georgia Tech campus facilities were shut down and thus manufacturing could not continue as the team was reliant on the resources available therein. The purpose and design of this test are described in this report, but without experimental results aerodynamic design decisions had to be based on extrapolations of CFD analysis. Additionally, without in-person meetings it was difficult to discuss and distribute required tasks, impacting the scope of the analysis presented here. Specifically, structural and component layout design was impacted as this requires detailed discussion among those most knowledgeable in the constituent subsystems to ensure robustness. In general, working efficiency was impacted since design tools normally available in campus facilities had to be accessed remotely if they could be accessed at all. Additionally, the productivity of required activities unrelated to the project, such as coursework and sponsored research, was negatively impacted, and so team members had less time to commit to this project than they otherwise might have.

Table of Contents

Acknowledgements	i
COVID-19 Disclaimer	ii
Table of Contents	iii
Table of Figures	v
List of Tables	vi
1 Introduction	1
2 Vehicle Configuration Trade Off Analysis	1
2.1 Requirements	1
2.2 Examination of different configurations	2
2.2.1 Conventional helicopter	2
2.2.2 Tandem	2
2.2.3 Segue	3
2.2.4 Tiltrotor	3
2.2.5 Quadcopter	4
2.3 Selection Process	5
2.4 Subsystem Configuration	7
3 Concept Sizing and Description	8
3.1 Overview of Sizing Process	8
3.2 Airscrews Sizing	9
3.3 Propulsion System Sizing	10
3.4 Structures Sizing	12
3.5 Controls Sizing	12
4 Geometry and Aesthetics	13
5 Aerodynamics	14
5.1 Airscrew Design	14
5.1.1 Baseline Simulation	15
5.1.2 RPM Study	17
5.1.3 Coning Study	17
5.1.4 Taper Study	17
5.2 Small-Scale Experiment	18
5.3 Vehicle Aerodynamics	19
6 Rotor	19
6.1 Aerodynamic Design Concept	19
6.2 Structural Design	21

7	Power and Energy	22
7.1	Mechanical Powertrain	22
7.2	Electrical Powertrain	22
7.2.1	Electric Power Technology	23
7.3	Propulsion Architecture Selection	24
7.4	Human Power	25
7.4.1	Maximum human power output	25
7.4.2	Mechanical to electrical power conversion and subsequent losses	26
7.4.3	Pedal-assist systems	26
8	Controls and Piloting	28
9	Flight Control System Concept	29
9.1	Equations of Motion	30
9.2	Yaw Control and Throttle	30
9.3	Roll and Pitch Control	31
10	Component Layout	32
11	Structures and Materials	33
11.1	Airframe Material	34
11.2	Airframe Design	34
11.3	Airscrew Material	34
12	Rotor and Airframe Loads	35
13	Structural Analysis	36
14	Concept Validation	37
15	Capability, Performance and Requirement Compliance	38
16	Maneuverability and Workload	39
17	Accommodation, Accessibility, Human Factors	40
18	Demonstrating Manufacturing and Feasibility	41
19	Project Summary	41
	References	43

Table of Figures

Figure 2.1	Conventional Rotor Layout Concept (Side-on)	2
Figure 2.2	Tandem Rotor Layout Concept (Side-on)	3
Figure 2.3	Segue Rotor Layout Concept (Side-on)	4
Figure 2.4	Tilt Rotor Layout Concept (Front-Back)	4
Figure 2.5	Quad-copter Rotor Layout Concept (Side-on, Skewed) . .	5
Figure 2.6	<i>Il Mulinello</i> system map	8
Figure 3.1	Flow chart of the vehicle sizing process	9
Figure 3.2	Powertrain flow diagram for the vehicle.	11
Figure 4.1	Rendering of <i>Il Mulinello</i>	13
Figure 5.1	Isosurface of Q-criterion for the baseline test case	16
Figure 5.2	Top-down view of surface pressure coefficient distribution for the baseline airscrew	16
Figure 5.3	Isosurface of Q-criterion for the high RPM test case . . .	17
Figure 5.4	Design of experimental test rig	18
Figure 5.5	Realized small-scale experimental test rig	19
Figure 6.1	Proposed rotor configuration based on aerodynamic analysis	20
Figure 6.2	Convergence history of thrust coefficient, power coeffi- cient, and figure of merit	21
Figure 6.3	CFD results for the dual airscrew geometry	21
Figure 7.1	Battery energy density trend and prediction	23
Figure 7.2	Shimano STEPS E8000 system on a bike (from Shimano's user manual)	28
Figure 8.1	Propeller control system	29
Figure 9.1	Diagram of the iterative control system for n iterations .	31
Figure 9.2	Cost of the calculated trajectory at each iteration for three different runs	32
Figure 9.3	Cost of the calculated trajectory at each iteration for dif- ferent learning rates	33
Figure 13.1	Airscrew FEA analysis results	36

List of Tables

Table 2.1	Pugh Matrix for rotor configuration	7
Table 4.1	<i>Il Mulinello</i> Details	14
Table 4.2	Bounding-Box Dimensions	14
Table 4.3	Main Rotor Aerial screws specifications	14
Table 4.4	Forward Propeller Aerial screws specifications	14
Table 5.1	Table of Airscrew performance CFD results	15
Table 7.1	Battery technology assumptions	24
Table 7.2	Electric Component technology assumptions	24
Table 7.3	Maximum work capacity in Watts (HP) from the NASA Data Book	26
Table 7.4	Shimano STEPS E8000 components information	27
Table 9.1	Table of variables for equations of motions	30
Table 11.1	Weighted Pugh matrix comparing possible airscrew mate- rial choices	35
Table 15.1	Table of variables for performance calculations	40

1 Introduction

Leonardo Da Vinci created machines that defied the imagination. One of his ambitions was to fly like the imposing hawks, who inspired his Great Kite flying machine. Motivated by Archimedes's screw, a screw that could pump water up, Da Vinci designed what would become the first machine potentially capable of vertical take-off and landing: the aerial screw (or airscrew), considered by many as the precursor of the modern helicopter, as attested by its presence in the cover of the Vertical Flight Society journal. While the aerial screw was not a feasible concept, it encouraged scientists to research the possibility of vertical flight. Despite the importance of the aerial screw in the vertical flight history, 500 years after its inventor's death, very little research has been made to study its technicalities and possible applications.

The Request for Proposal (RFP) for the 37th Annual Student Design Competition, sponsored by Leonardo, has created an incentive to increase the body of knowledge concerning the aerial screw. The aim of this report is to present a VTOL vehicle based on Leonardo's aerial screw concept, capable of sustaining flight over at least twenty meters and carrying one passenger. To respond to the RFP, this team presents *Il Mulinello*, a tandem bike powered by two pairs of coaxial airscrews and one forward propeller airscrew. The vehicle design was created from the study of the aerial screw main aspects, using its strengths and solving its defects, while trying to keep as loyal to Da Vinci's initial idea as possible.

2 Vehicle Configuration Trade Off Analysis

The first task the team encountered was choosing the vehicle configuration. To do so, the mission requirements were analyzed and juxtaposed to the original aerial screw design. After determining which characteristics had to be prioritized, the team studied different configurations and chose a final design.

2.1 Requirements

At its heart, the goal of the team's design efforts sought to take Da Vinci's aerial screw concept and apply to it modern methods of design an analysis in the hopes of reaching a greater level of understanding behind the physics that drive such a concept as well as developing a modern re-imagining of a historical engineering landmark. The RFP defines an aerial screw (or "airscrew") as a single-bladed rotor with solidity equal or greater than one with a continuous surface. This definition is explored in further detail in subsection 6.1. The vehicle must produce the majority of its lift and thrust utilizing airscrews and must be capable of carrying one pilot or passenger weighing at least 60 kg. In addition, the RFP defines a mission consisting of a vertical take-off, followed by a five-second hover at an altitude of at least 1 meter. The vehicle must then cover a minimum distance of 20 meters, hold the hover position for another five

seconds, and land vertically.

2.2 Examination of different configurations

Five rotor configurations were considered in the context of creating a modern airscrew: a conventional single-rotor configuration, a tandem rotor configuration, a segue-like configuration, a tilt-rotor configuration, and a quad-rotor configuration.

2.2.1 Conventional helicopter

The first design considered was the traditional helicopter, with a single main rotor and a tail rotor. The single main rotor would be an airscrew, contributing to lift and thrust, while the tail rotor could be either a traditional rotor or an aerial screw, and is used for torque balance and yaw control. Roll and pitch controls are achieved by tilting the main rotor thrust.

A single main airscrew makes the configuration similar to the original Da Vinci concept, but the addition of a tail and a tail rotor makes the two configurations extremely distinct.

This configuration is simple, relatively low-cost, and presents lower risks than other configurations. However, the tail rotor absorbs power and doesn't contribute to lift or thrust, therefore increasing the vehicle power requirement [1]. When choosing the configuration, the thrust produced by an airscrew was still unknown, but the team expected it to be considerably lower than the thrust produced by a regular low-solidity rotor while producing significantly more torque. As such, significantly more power would need to be directed towards the tail rotor to provide counter-torque. This additional power requirement was therefore undesirable. Moreover, adding a swash plate to the airscrew increases the complexity of the design.

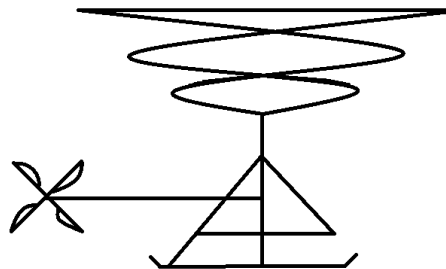


Figure 2.1 Conventional Rotor Layout Concept (Side-on)

2.2.2 Tandem

The tandem configuration consists of two rotors rotating in opposite directions located fore and aft of the vehicle in similar fashion to Boeing's Chinook. Both

rotors would be airscrews, and provide the lift and thrust requirements of the vehicle. With two counter-rotating main rotors, torque balance is inherent and no tail rotor is required. The increase in power requirement seen in the traditional helicopter configuration is therefore avoided. The use of airscrews as main rotors on this configuration presents similar control challenges to the conventional rotor configuration with additional challenges for yaw control. This configuration offers an innovative concept, while keeping the initial airscrew look.

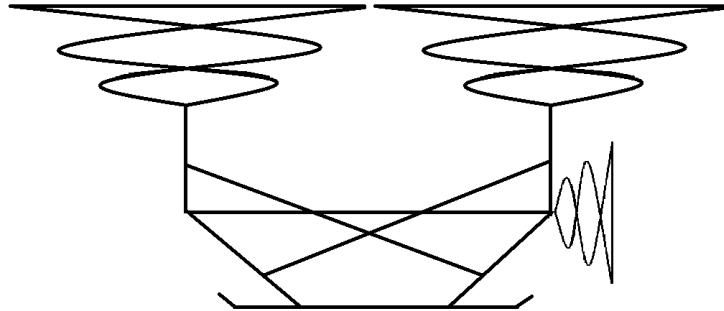


Figure 2.2 Tandem Rotor Layout Concept (Side-on)

2.2.3 Segue

The “Segue” design configuration takes inspiration from the proprietary two wheeled vehicle of the same name (stylized as “Segway”). The wheeled version operates as a sort of inverted pendulum, utilizing electric motors and tilt sensors for control of motion.

The proposed configuration will utilize a single airscrew rotor located along the pitch axis of the vehicle with the occupant standing to operate the vehicle in a similar manner to the wheeled Segway by leaning to move forward using a gyroscope which would also provide counter-torque. The unprecedented nature of this design presents new control and stability challenges.

While an interesting concept and would result in a vehicle that is fairly light with a low footprint, this configuration provides a heavy control system challenge to manage both forward flight and altitude control using just pitch adjustments.

2.2.4 Tiltrotor

The tiltrotor design allows to takeoff vertically, and transition to forward flight. The hybrid configuration between a conventional helicopter and an airplane allows for a higher forward speed than a conventional helicopter [2]. This feature is however not a priority due to the low range requirement of the vehicle. The tiltrotor design has a more complex aerodynamic design than a conventional

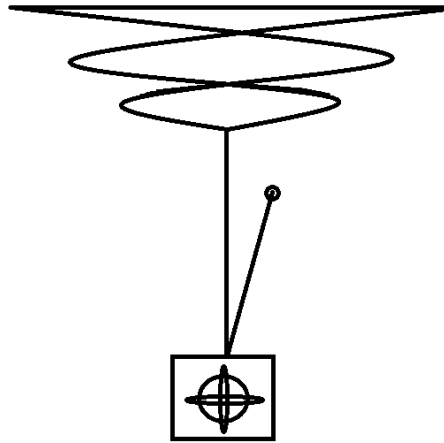


Figure 2.3 Segue Rotor Layout Concept (Side-on)

helicopter. Moreover, smaller rotor diameters mean that for the same gross weight, the tiltrotor will have a higher disk loading than the conventional helicopter. Lastly, the downwash of the rotors on the wings decrease the hovering efficiency of the aircraft. This problem can be solved by using tiltwings, to tilt both the rotor and the wings. However, this increases the complexity of the mechanism, and increases the weight, as it requires additional tilting actuation systems.

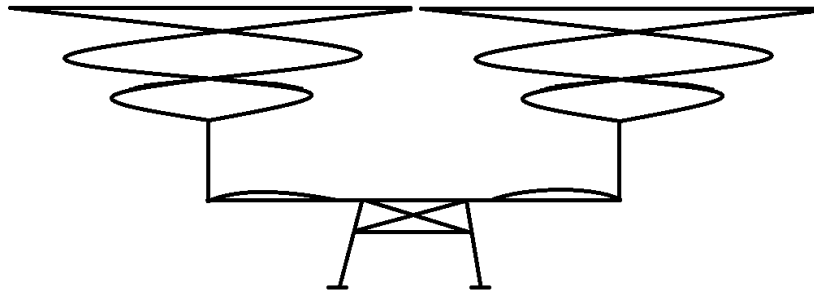


Figure 2.4 Tilt Rotor Layout Concept (Front-Back)

2.2.5 Quadcopter

The quadcopter configuration proposal takes inspiration from the typical unmanned small drone, consisting of four airscrews placed at each corner. This design configuration would provide unmatched control and stability characteristics however at a cost of vastly increased complexity and power requirements. Given the likely low efficiency of the airscrew design, having a minimal number

of rotor systems is optimal to maintain the smallest power requirements.

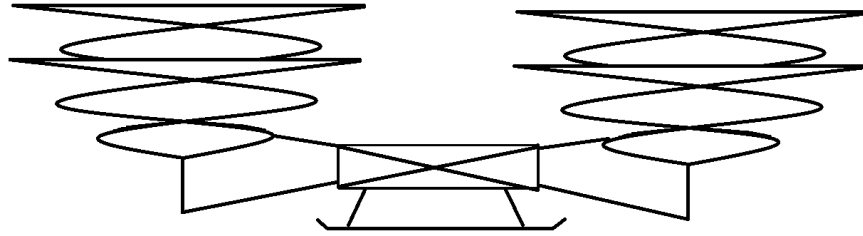


Figure 2.5 Quad-copter Rotor Layout Concept (Side-on, Skewed)

2.3 Selection Process

To determine which configuration suited this project, the requirements outlined in the RFP were evaluated to determine the selection criteria the team would use. From preliminary studies of airscrew aerodynamics, the team knew the power requirement would be critical. Indeed, the figure of merit of an airscrew is much lower than for a conventional rotor of lower solidity. Therefore, the power required for each configuration was an important criteria. The RFP notes that the aircraft should be reminiscent of Leonardo Da Vinci's aerial screw. As such, aesthetics of the configuration, and its similarities with the original concept, were considered an important selection criteria. The ease of control and piloting, in addition to safety of the pilot, were considered as another important selection criteria. Lastly, the cost of manufacturing of the aircraft was taken into consideration.

Table 2.1 is a Pugh Matrix describing the expected ability of each configuration to meet needs in categories chosen based on the requirements outlined in the RFP with appropriate weight factors. As the power required was an imperative for the success of the mission, it was given the most weight. The RFP's goal is to explore the aerial screw concept. As such, the team decided that aesthetics, and therefore the configuration similarity with Da Vinci's design, should also have a large weight. It needed, however, to be lower than the power required, since, as stated above, power is a must. To achieve the mission, control of the vehicle was important. It was therefore given a slightly lower but similar weight than the aesthetics. Lastly, the team decided to give cost and safety the same weight, lower than the other criteria. Indeed, cost is not a priority in this design. This concept aims to be innovative and explore the possibilities of an airscrew-powered vehicle, providing a demonstrator more than a passenger vehicle. As such, safety and cost were given lower weights, but remained important factors when selecting the configuration.

Each criteria was given a score between 1 and 5, 5 being the most desirable and 1 the least desirable. Each weighted criteria score was then summed, giving the final score for each configuration.

The power requirement scores were obtained from each configuration analysis. The scores were low for all configurations, as the aerial screw is not efficient. Moreover, the score was lowered for tilt-rotors and seguey, as these configurations require smaller radii for the same gross weight, and therefore lower the power efficiency. The quadrotor, requiring even lower radii, obtained the lowest power required score.

The aesthetics scores were necessarily subjective. Indeed, the definition of aesthetics can vary from person to person. The team scored based on the resemblance of each configuration to the original design by Leonardo Da Vinci and the prominence of the airscrew in the design. Also, more innovative concepts were scored more highly in this category. The conventional helicopter, while keeping the single main rotor vision, had a lower score due to the tail required to balance the main rotor torque and the lack of room for innovation. This tail was considered by the team as penalizing, as the design clearly deviated from Da Vinci's drawing. The team decided that despite the desire to stay as close to the original design as possible, at least two main rotors were necessary so that the torque balance could be achieved. Adding a second main rotor would, however, deviate from the single-rotor design envisioned by Da Vinci. Therefore, no aesthetics score was rated as 5. Configurations exhibiting the closest resemblance, with two main rotors, were given the higher score: the tandem, the tilt rotor and the segue.

The control and safety scores were greatly tied together. The quadrotor was given the highest control score. Indeed, with four rotors, this configuration allows for an easier control of all degrees of freedom. Moreover, control systems for quadrotors are vastly available, and the complexity of the design is therefore lowered. For the same reasons, along with the possibility of favorable pilot positioning, the quadrotor was given the higher safety rating. The conventional helicopter was given the second highest control and safety scores. This configuration, being the most commonly used, is known and the control system is easy to implement. The presence of a tail rotor also provides simple yaw control. However, a conventional rotor uses a swash plate to tilt the main rotor, which would be hard to achieve with an airscrew. The segue, never implemented in an aircraft, is a non-minimum phase system, inherently unstable. This unstable behavior, coupled with the lack of previous work on this configuration, led the team to rate the segue with a low control score (but non minimum, as a non-minimum phase control is possible), and a minimum safety score. The tilt rotor obtained the same scores as the segue, but for different reasons. Tilt-rotors, as detailed in the previous sections, have an increased complexity. Adding tilting mechanisms to the configuration makes the failure rates higher, and can lead to a harder to control system. Lastly, the tandem configuration was given a slightly higher control rating than the segue and the tilt-rotor, but still a lower score than a conventional helicopter. Indeed, the tandem configuration still includes a complicated roll and pitch control, since a swash plate is hard to implement on an aerial screw, and is not as researched as conventional helicopters.

The cost scores were obtained by evaluating the expected weight, complexity, and innovation of each configuration. Indeed, a completely new design requires

	Weight	Tandem	Conventional	Tilt	Quad	Segue
Power Required	8	3	3	2	1	2
Cost	1	3	3	1	1	2
Aesthetics	3	4	2	4	1	4
Control	2	3	4	2	5	2
Safety	1	2	4	1	5	1
Total		47	45	34	27	35

Table 2.1 Pugh Matrix for rotor configuration

research and more rigorous testing, increasing the cost of the project. The tilt rotor, using a complex turning mechanism as explained before, has the higher cost, while the tandem and conventional configurations are less costly.

As shown in Table 2.1, the tandem configuration obtained the highest score, and was therefore chosen to answer to the RFP.

2.4 Subsystem Configuration

Upon the selection of a rotor configuration, a list of critical subsystems was generated and a process for the design, selection, and sizing of each of these components was determined. These subsystems are:

1. Main Rotors
2. Front Propeller
3. Turning System
4. Power Storage
5. Power Distribution
6. Motors
7. Airframe
8. Pilot Interface
9. Control System

The system map shown in figure 2.6 describes how each subsystem interacts with the other subsystems and helped guide decisions for the placement, priority, and design of each subsystems. The main rotors are responsible for generating lift and giving the pilot altitude control. The front propeller is responsible for generating thrust and giving the pilot velocity control. The turning system was responsible for giving the pilot attitude control. The power storage system is responsible for ensuring the ability of *Il Mulinello* to meet the mission requirements. The power distribution system is responsible for distributing power to the motors according to pilot throttle inputs. The motors are responsible for

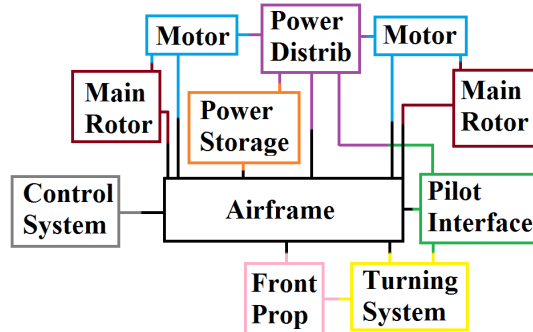


Figure 2.6 *Il Mulinello* system map

supplying power to the main rotors. The airframe is responsible for ensuring the structural integrity of *Il Mulinello*. The pilot interface gives the pilot altitude, attitude, and velocity control and ensures the pilot's safety and comfort. The control system ensures vehicle stability. The design and selection of the subsystems are described in their respective sections.

3 Concept Sizing and Description

In this section, the process and analyses for sizing the subsystems is discussed. The vehicle's aerodynamics, propulsion system, structure, and controls system are evaluated to meet the mission requirements and close the vehicle. The pilot is fixed so the vehicle was sized with the specified mission and essentially a 60 kg (132 lb) payload. The propulsion system weight, which includes the airscrews, is 137 kg (302 lb) and makes up a majority of the vehicles weight. The structure and controls system, which includes the turning mechanism, are similar in weight at 26.5 kg (57.3 lb) and 20.9 kg (44 lb) respectively. With the addition of the pilot, this brings the total weight of the vehicle to 244.4 kg (537.9 lb).

3.1 Overview of Sizing Process

A typical iterative sizing approach was implemented for sizing the vehicle. This approach breaks the vehicle down into systems which are connected in the process and sized during each iterative loop. Some systems, such as the airscrews and propulsion system are further broken down in components which are sized within each loop as well. An initial guess of the total vehicle weight is used to begin the sizing process. This is fed to the aerodynamics and airscrews so that they can be sized to provide enough lift to keep the vehicle in hover. This power requirement is then fed to the propulsion system which propagates the power requirement through each of the components inside the powertrain. Components are sized based on the power required upstream of them and an estimate of their

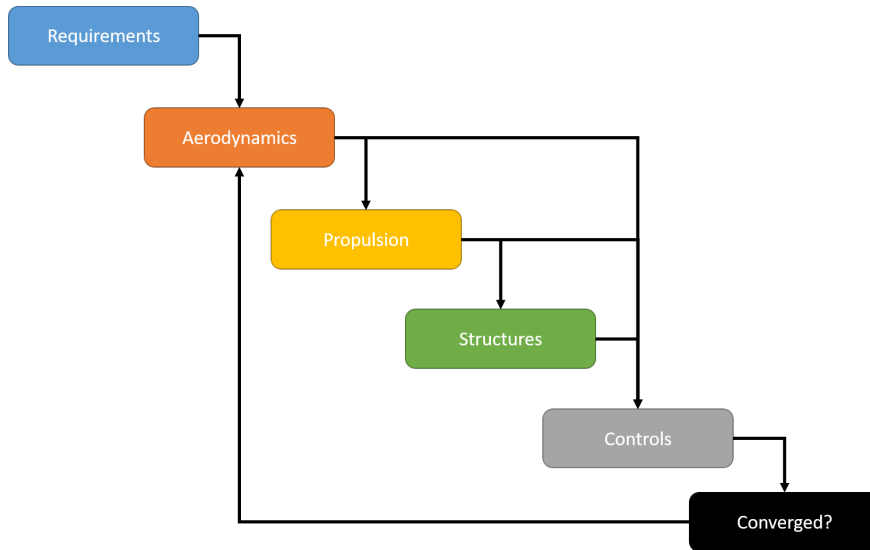


Figure 3.1 Flow chart of the vehicle sizing process

specific power and efficiency. The next system to be sized is the structure of the vehicle which is sized to be able to support the vehicle through different loading conditions throughout the mission. The final system to be sized is the control system which consists of deflectable flaps which interact with the airscrew wake and allow for roll and pitch control. Figure 3.1 shows the flow of information during the sizing process as each system of the vehicle is sized and the vehicle size is converged.

More detail on the specific sizing of each system is described in the following section. The pilot and human powered system are assumed to be constant as they are not expected to change during the sizing of the vehicle. This fixed payload and the mission determine how large the vehicle will need to be based on the assumptions made in the vehicle design and sizing. Once each system is sized initially, a new total vehicle weight is calculated based on the sum of the systems and is compared to the original guess. A new guess value is calculated based on the difference of these two value and the process is repeated until the guess weight and the calculated weight are equal within a predetermined tolerance.

3.2 Airscrews Sizing

By generalizing results from a computational fluid dynamics (CFD) study of the dual airscrew geometry, it was possible to determine the radius and power requirement of the two airscrews given a thrust requirement. Equation 1 describes how the radius R can be chosen based on the thrust requirement T if the tip speed U_{tip} is prescribed. Once the radius was chosen, the power re-

quired P to run the airscrew was given by equation 2. In these equations, the thrust coefficient C_T and the power coefficient C_P come from CFD analysis of a chosen airscrew geometry. Equation 3 describes how the mass of the airscrew m was determined given a root cutout radius R_0 , material density ρ_s , material thickness t_s , and pitch ratio h for the chosen airscrew geometry. The airscrew geometry can be thought of as a series of sectional helices with linearly varying taper ratios. The length of these helices can be integrated and multiplied by the material thickness and density to get the mass of the airscrew. Since each main rotor consists of two coaxial airscrews, the integrated mass is doubled.

$$R = \sqrt{\frac{T}{\rho\pi U_{tip}^2 C_T}} \quad (1)$$

$$P = \rho U_{tip}^3 \pi R^2 C_P \quad (2)$$

$$m = 2\rho_s t_s \int_{R_0}^R r \sqrt{4h^2 + \pi^2 \left(2 - \frac{r - R_0}{R - R_0}\right)^2} dr \quad (3)$$

3.3 Propulsion System Sizing

The propulsion systems is sized in order to provide enough power to the thrust sources to keep the vehicle in hover. The system is made up of several parts which all need to be sized according to this power. The main parts of the propulsion system are the vertical airscrews which provide the lift, the motors required to power those airscrews, the powersplit unit which controls the power going to each airscrew and allows for variable RPM of the forward and aft screws, and the battery which stores the energy that powers the other elements. In order to size the components appropriately, the power requirements are analyzed from the top of the powertrain (the airscrews) down to the bottom of the powertrain (the battery) as this allows for efficiencies to be considered relatively easily. Figure 3.2 shows the powertrain architecture used for the propulsion system.

The power requirements for each component are determined by following the flow mentioned before (from thrust source to energy source in this case). Each component, with a slight exception for the battery, is sized in a similar way. The component power requirement is first calculated by using Equation 4 below which takes the power requirement upstream of the component and the component's efficiency η_i to calculate the power required $P_{req,i}$ for the specific component.

$$P_{req,i} = \frac{P_{upstream,i}}{\eta_i} \quad (4)$$

The component's required power and specific power are then used to calculate the component's weight W_i using Equation 5 below.

$$W_i = \frac{P_{req,i}}{\xi_i} \quad (5)$$

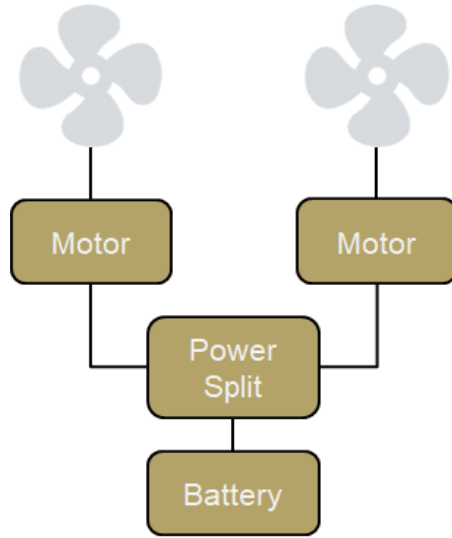


Figure 3.2 Powertrain flow diagram for the vehicle.

Finally, after each component is sized, the weights of each component are added together to get the total propulsion system weight W_{Sys} as per Equation 6

$$W_{Sys} = \sum_i^n W_i \quad (6)$$

As mentioned, upstream power required for the airscrews is calculated so that the thrust provided by the airscrews will balance the weight of the vehicle. The specific power of the airscrew is calculated based on the weight and power estimates described previously. Moving down the powertrain, the motors are next to be sized and the power requirement for these components is simply the power requirement of the airscrews divided by the motor efficiency and so on for each component. The final component of the powertrain is the energy source, the battery. The battery is sized in two ways and the most constraining case is taken to ensure the mission can be completed and that the vehicle can maintain hover. Sizing the battery is first done in terms of the power requirement, again in a similar manner to the previous components by using the power requirements upstream, the efficiency, and the specific power. The second sizing method for the battery uses the specific energy and the energy required to fly the mission. This provides a practical approach and allows the team to determine which kinds of battery cells would be most beneficial in reducing the overall weight of the vehicle. Different battery cells are suited for different purposes, for example a more power dense cell will have a lower energy density than one designed for energy density specifically. By considering both energy and power sizing of the

battery an optimal battery cell can be chosen such that the battery weight is minimized and thus so is the weight of the vehicle.

3.4 Structures Sizing

Developing an airframe for a manned vehicle requires striking a key balance between human factors and structural optimization. The difficulties of designing such a system are amplified by the experimental and lightweight nature of the vehicle and great care must be taken to ensure that every curve, brace, and beam are implemented with efficiency in mind. To begin sizing the airframe, an understanding of the configuration and payload requirements of the vehicle must first be reached. From these requirements can be derived a rough estimate of the vehicle's weight as well as the weight of the components. This will allow for a rough estimate of how each component must be located in order to ensure optimum balance. Perhaps the largest driving factor in the size of the airframe is the diameter of the airscrew blades required to produce the necessary thrust based on the estimated weight of the entire loaded vehicle. The diameter of the blades creates a lower bound for the length of the airframe and determines the positioning of the motors. From there, additional length will be added to make room for components or to make improvements in occupancy space. Determining the location of the airscrews first and foremost is crucial to developing the force and moment profile that the frame will see. Using these estimated loads with a healthy factor of safety, Finite Element Analysis (FEA) can then be utilized to determine weak points in the structure as well as identify areas where the structure can be trimmed to reduce weight and improve efficiency. To calculate the weight of the structures, material properties are used. However this process requires user input and human interaction and is very inefficient to do in each iteration of the sizing process. To circumvent this, several points are chosen to size the frame weight using a lower and upper bound, allowing the sizing process to interpolate a weight. This provide a simple way to size the structure and removes the requirement of user intervention.

3.5 Controls Sizing

The centerpiece of the control system consists of the four flaps that will be used for pitch and roll control. These flaps take advantage of the wake of airscrews to carefully direct flow in such a way that will produce desired rotations of the vehicle. Given the difficulties in understanding the aerodynamic effects of an airscrew, the sizing of these flaps must begin with a very rough first estimate. From there, using the dynamics of the vehicle, the effective range of deflection angles necessary to achieve the desired performance characteristics are determined. These deflection angles must be looked at in the context of the capabilities of the actuation system design as well to ensure they do not exceed the loading or extension limits and if the system is capable of making fine enough deflections required to maintain stability in both static and dynamic cases. The flaps are positioned in the same x-y plane as the center of gravity of

the vehicle to ensure that there are no secondary effects when they are deflected. As a starting point, the flap surface area was chosen to be 0.01 square meters. With the weight estimates of the current iteration, the moments of inertia and thrust are calculated and input into the control system model for sizing. The flaps have two degrees of freedom in the sizing process, the physical size and the horizontal distance from the center of gravity and a solution is chosen such that control surfaces are adequate for the required vehicle maneuvers. At each weight sizing iteration, the feasibility of the deflections is evaluated, and if needed, the flaps are resized.

4 Geometry and Aesthetics

A unique component of the RFP was the inclusion of a soft requirement that the vehicle should in some way resemble the airscrew design of Leonardo Da Vinci. The team interpreted this to mean that the size of the vehicle and the proportions of the airscrew should be close to those implied by Da Vinci's drawing. As such, the geometry of *Il Mulinello's* airscrews were limited to linearly tapered helices, and the vehicle was sized to be as small as possible while supporting the weight of a human. Additionally, it was decided that the inclusion of human-generated power was a key component of evincing the spirit of Da Vinci's vehicle. While humans are not capable of generating enough power to provide sufficient lift to support their own weight using a rotor as inefficient as the airscrew, a human could provide enough power to control the forward motion of the vehicle. Thus, this became a primary component of *Il Mulinello's* design. Tables 4.1-4.4 describe the major parameters of *Il Mulinello's* geometry.



Figure 4.1 Rendering of *Il Mulinello*

Configuration	Tandem bike
Payload	1 Pilot, 60 kg (132 lb)
Gross weight	245 kg (540 lb)

Table 4.1 *Il Mulinello* Details

Length	3.04 m (9.97 ft)
Height	2.17 m (7.11 ft)
Width	1.72 m (5.64 ft)

Table 4.2 Bounding-Box Dimensions

Maximum diameter	1.72 m (5.64 ft)
Taper Ratio	0
Number of Revolutions	2
Solidity	1

Table 4.3 Main Rotor Aerial screws specifications

Maximum diameter	1.22 m (4.00 ft)
Taper Ratio	0
Number of Revolutions	2
Solidity	1

Table 4.4 Forward Propeller Aerial screws specifications

5 Aerodynamics

This section begins the discussion of the analysis and design techniques used to create *Il Mulinello*. As a flying vehicle, aerodynamic analysis played a critical role in determining the capabilities and performance of a vehicle which uses airscrews for the main rotor geometry. Inspection of the mission requirements established a limited range of aerodynamic conditions which *Il Mulinello* would encounter, and so aerodynamic analysis could be focused on these scenarios. Of these, hover and very-low-speed forward flight form the majority, enabling very detailed analysis of these conditions.

5.1 Airscrew Design

The biggest unknown when approaching this concept was the aerodynamic performance of an airscrew. Very few if any detailed and rigorous studies have been performed on such a rotor geometry. This was part of the motivation to constrain the mission to hover and very low-speed forward flight. As such, primary aerodynamic analysis could be limited to hover performance calculation and optimization with further investigation into forward-flight effects. The first

	Thrust Coefficient	Power Coefficient	Figure of Merit
Baseline	0.0090	0.00459	0.1321
High RPM	0.0081	0.00540	0.0963
Upward Coning	0.0087	0.00459	0.1259
Downward Coning	0.0086	0.00455	0.1240
Taper	0.0056	0.00180	0.1655

Table 5.1 Table of Airscrew performance CFD results

attempts at characterizing the aerodynamics of an airscrew involved a rough estimation of the power requirement by integrating a flat-plate drag profile over the surface of the airscrew. The results of this were used to inform power requirements for a small-scale experiment as well as for the full vehicle. Clearly, however, higher fidelity analysis was needed before the design of the main rotors could progress. A simple CFD study was designed in which the effects of various geometric parameters of an airscrew on hover performance were examined. The parameters studied were the taper ratio ($t = \frac{R_1}{R_2}$), the coning angle, and the rotor speed. The results of this study are shown in table 5.1. From this table one can conclude that increasing the RPM reduces the efficiency of the airscrew in hover, that applying a coning angle has a small detrimental impact on hover efficiency, and that a taper ratio above unity significantly improves hover efficiency.

5.1.1 Baseline Simulation

The baseline case for the CFD study consisted of a 0.15 meter (6 inch) radius single-bladed airscrew with a 0.02 meter (three-quarter inch) diameter shaft through the center. The baseline airscrew had a taper ratio of 1, no coning angle, and a pitch of 0.075 meter (3 inches). This was designed to match the proposed geometry of the small-scale experiment for easy comparison between the two studies. The computational domain was discretized with a single-block unstructured finite-volume grid with 5 million nodes and solved using the NASA CFD code FUN3D. The airscrew was spun for 2 revolutions at sea-level conditions such that the tip mach number was 0.44. The flow equations were solved first-order accurate in time with a time step corresponding to a quarter degree azimuth angle rotation and second-order in space. Important results of this baseline study included the structure of the wake shown in 5.1 where an isosurface of Q-criterion shows how the tip vortex remains above the outer edge of the airscrew, as well as the pressure distribution showing how the majority of the lift is generated at the leading edge of the airscrew, described in figure 5.2. It was also noted that the tip vortex generates favorable pressure on the upper surface around the tip of the airscrew.

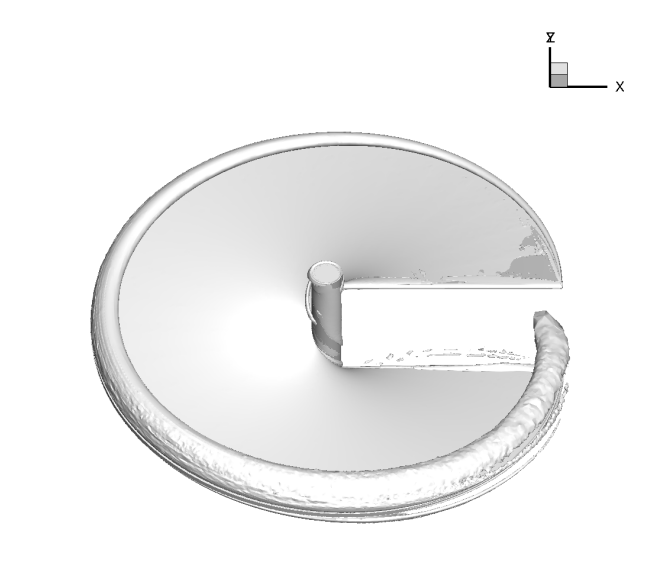


Figure 5.1 Isosurface of Q-criterion for the baseline test case

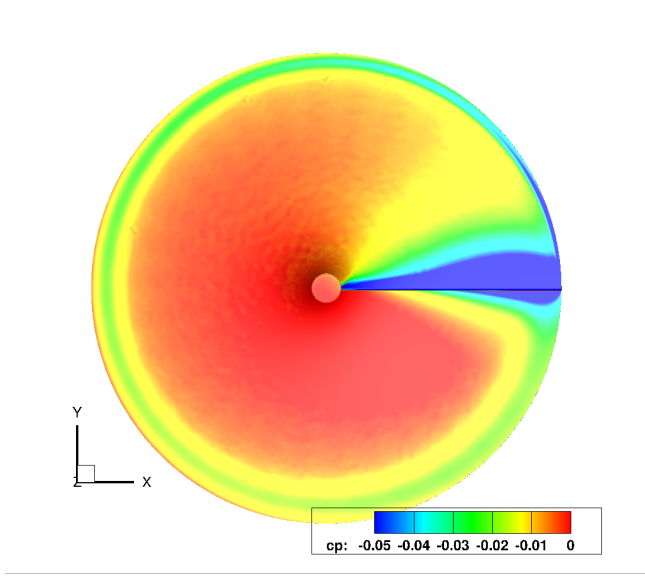


Figure 5.2 Top-down view of surface pressure coefficient distribution for the baseline airscrew

5.1.2 RPM Study

A simulation using the baseline geometry was run with a tip mach number of 0.66, corresponding to a 50% increase in the RPM of the airscrew. This had the effect of reducing the thrust coefficient and greatly increasing the power coefficient, representing a significant loss of aerodynamic efficiency in hover. This was attributed to the leading-edge separation present at the tip of the airscrew seen in figure 5.3. It can be deduced that increasing the RPM, while increasing the amount of dimensional thrust produced, comes at a cost of efficiency. Thus it is desirable to find alternative methods for increasing thrust before increasing the RPM.

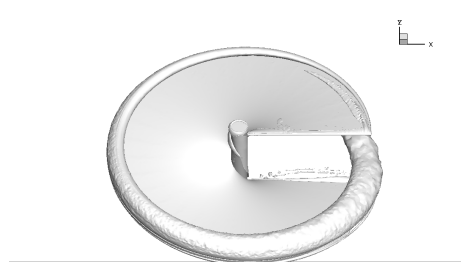


Figure 5.3 Isosurface of Q-criterion for the high RPM test case

5.1.3 Coning Study

In order to study the effects of coning on the aerodynamic performance of an airscrew, altered geometry with a 10 degree coning angle was used to generate a new computational grid which was run at the baseline conditions. Positive and negative coning angles were simulated by spinning the altered geometry both clockwise and counter-clockwise and measuring the thrust and power generated in the appropriate directions. Coning had a small detrimental effect on the thrust generation, likely due to the inward/outward skew of the lift vector without much effect on the power requirement. This opened up coning as an option to increase structural strength.

5.1.4 Taper Study

Finally, the effects of taper were studied by creating a new geometry with a taper ratio of 0.5 and running the new grid at the baseline conditions. While the thrust was reduced with this geometry, the power requirement was greatly reduced, resulting in a much higher figure of merit for hover efficiency. This is due to a reduction in the “inactive area” where lift is not being produced and which only contributes drag. If a solidity of one could be maintained, it was clear that applying taper to the airscrew would significantly increase its flight capabilities.

5.2 Small-Scale Experiment

In order to make robust design decisions, detailed performance metrics were required beyond what was feasible with a CFD study. A small-scale experimental study was therefore planned in which thrust generation would be measured against power and RPM for various airscrew geometries. The design of the test rig for this experiment is shown in figure 5.4. The design included an adjustable bearing to accommodate various shaft lengths, a motor mount, a rotating moment arm, and a load cell which would measure the thrust. Shafts could be interchanged quickly by making use of the fixed motor and bearing adapters, allowing for rapid testing of different geometries. The airscrew geometries were to be defined using spokes with varying lengths, positions, and angles to create airscrew taper, pitch, and coning, respectively. The spokes were connected by cardboard panels which fully resolved the desired airscrew surface geometry. The motor was able to monitor power output and RPM, allowing for easy correlation between these metrics and thrust produced. The test rig and airscrew shafts were machined out of aluminum using a lathe and drill press for the shafts and a water jet to cut the pieces of the test rig. Manufacturing reached the stage shown in figure 5.5, where the airscrews and the majority of the experimental test rig were built when Georgia Tech campus facilities were shut down due to the COVID-19 pandemic. As such, manufacturing came to a halt and the experiment was postponed indefinitely.

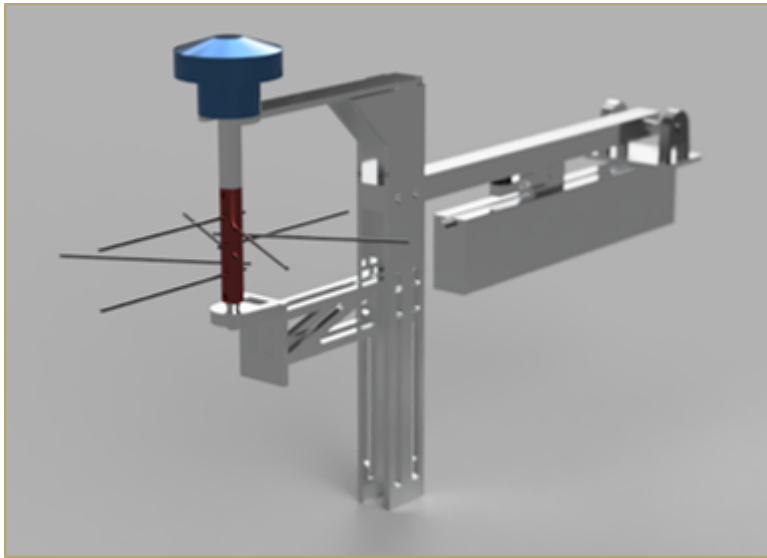


Figure 5.4 Design of experimental test rig

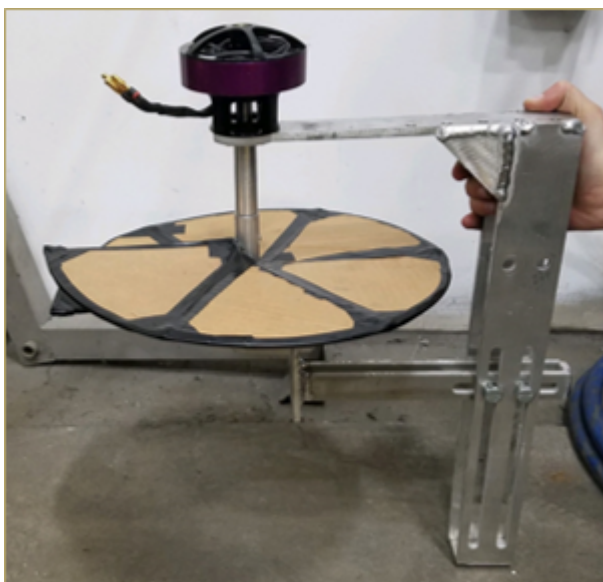


Figure 5.5 Realized small-scale experimental test rig

5.3 Vehicle Aerodynamics

Due to the very-low-speed flight conditions *Il Mulinello* was expected to encounter, vehicle aerodynamics did not play an important role in the overall design. For range and endurance calculations, *Il Mulinello* could simply be treated as a bluff body and was still more than capable of meeting mission requirements.

6 Rotor

6.1 Aerodynamic Design Concept

The parametric airscrew CFD study resulted in two major take-aways: first, that an airscrew rotor needs to be geometrically balanced in order to prevent extreme vibratory loads due to the concentration of lift at the leading edge, and second, that an ideal design must take advantage of the efficiency of high taper ratios. To address the first problem, a coaxial airscrew concept was designed, in which two single-bladed airscrew would share the same shaft with an offset of 180 degrees azimuth angle. This allowed for potentially perfect weight and lift balancing due to the geometric symmetry of the design. Before the second problem could be addressed, a rigorous definition of solidity needed to be chosen to determine whether a proposed design met the requirement of having a solidity of at least one. The definition of solidity for a general blade geometry according to reference [2] is given in equation 7. The solidity distribution for a tapered

airscrew blade is given in equation 8, assuming that taper ratio t is linearly applied from the leading to the trailing edge over n revolutions. Integrating equation 8 according to equation 7, the expression for the solidity of a tapered airscrew is given in equation 9. This allowed for the choice of a combination of n and t such that the design could take full advantage of taper while also meeting the requirements. The minimum possible taper ratio was, of course, 0, for which two revolutions were required to meet the solidity requirement. This resulted in an airscrew design which looks geometrically similar to that shown in figure 6.1 with freedom to scale the radius, apply coning, and adjust the pitch according to geometric, structural, and lift requirements, respectively. Note that it was possible to apply a much more complex taper function in such a way as to approximate a conventional rotor blade, greatly improving the efficiency of the rotor over a linearly tapered design. However, this was determined to be not in the spirit of the RFP, and so design optimization was limited to linearly-tapered airscrews.

$$\bar{\sigma} = \int_0^1 \sigma(r) dr \quad (7)$$

$$\sigma(r \leq t) = n, \quad \sigma(r > t) = n \left(1 - \frac{r-t}{1-t} \right) \quad (8)$$

$$\bar{\sigma} = \frac{n}{2}(1+t) \quad (9)$$

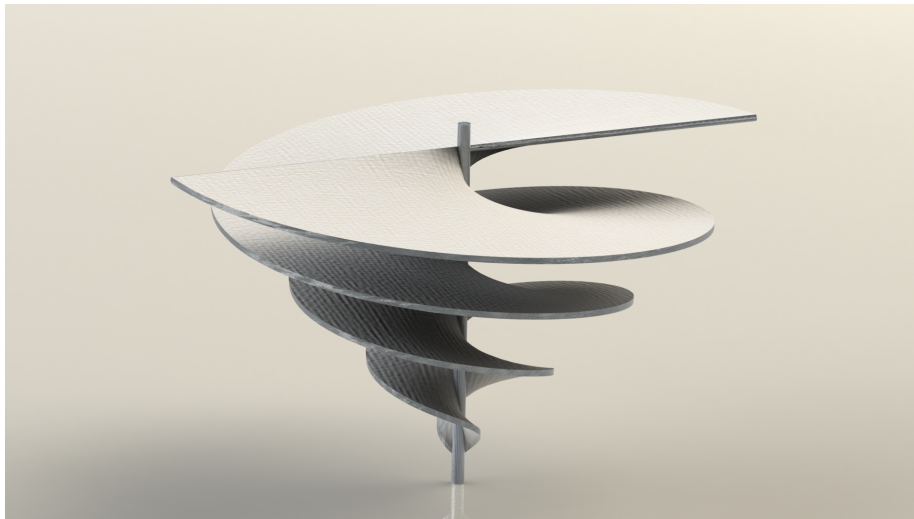


Figure 6.1 Proposed rotor configuration based on aerodynamic analysis

This new geometry was analyzed using the same CFD setup at a tip Mach number of 0.7 and a radius of 1.22 m (4 ft) with a pitch ratio of 0.5. This

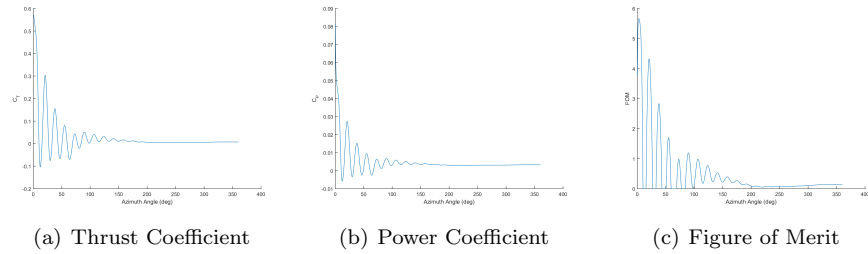


Figure 6.2 Convergence history of thrust coefficient, power coefficient, and figure of merit

produced a thrust coefficient of 0.0073 at a power coefficient of 0.0032716, giving a figure of merit of 0.13373. These were the numbers used to size the main rotors and forward propeller. Convergence histories of these metrics are given in figure 6.2. The unsteady wake geometry is shown in figure 6.3(a) as an isosurface of Q -criterion. The pressure distribution is shown in figure 6.3(b), which illustrates how the dual-aircrew design balances the aerodynamic forces around the axis of rotation.

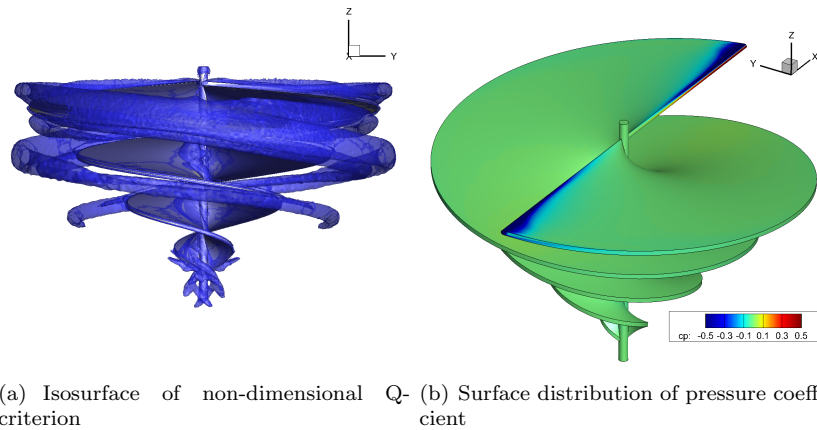


Figure 6.3 CFD results for the dual aircrew geometry

6.2 Structural Design

The dual aircrew's structural properties were also assessed using static FEA in order to determine what material and blade properties are required for structural integrity. This analysis is further expanded upon in section 13.

7 Power and Energy

With a better understanding of the expected efficiency of an airscrew rotor, design and analysis of various power systems could be performed and an appropriate system could be chosen given the mission requirements. This section describes the design and analysis performed and the chosen configuration for the power system design.

7.1 Mechanical Powertrain

If the energy source was to be fuel, the power would need to be provided by an internal combustion engine given the size of the vehicle. Due to the estimated engine size, the engine efficiency was likely be quite low, requiring more fuel as compared to larger internal combustion engines. In order have proper linkage between the engine and the airscrews, a free power turbine would need to be used to extract work from the engine. The airscrews would need to rotate in opposite directions to avoid stability issues caused by their torque. This could be accomplished by having the engine sit somewhere in between the two airscrews so that a shaft is extended out either end of the engine. Using conical gearing, the shaft power can be transmitted upward for each airscrew allowing them to spin in opposite directions. This has a drawback, however, because the two airscrews would either need to rotate at the same RPM or additional gearing would be needed to vary the RPM. Additional gearing would be more complex and add weight to the powertrain in addition to taking up valuable room.

The mechanical powertrain also poses another problem that is less straightforward; sizing the engine during the vehicle sizing process. Simply applying a power-to-weight ratio does not work because turboshaft and reciprocating engine scaling cannot be extrapolated very much. A more accurate way to properly capture the major sizing effects is to rubberize several engines of different size classes and use a piece-wise approach based on power requirements. The fuel burn and losses will not be captured accurately if these sizing effects are ignored. This adds significant complexity in the vehicle sizing and requires accurate models of the engines and their scaling parameters which is not favorable.

7.2 Electrical Powertrain

A battery powered system is a bit more flexible in terms of locations of powertrain components. Batteries can take many different forms and can be placed almost anywhere in the vehicle allowing for more variety in terms of the architecture layout. To provide power to the airscrews, motors needed to be used to transfer the electrical energy to mechanical power. Each airscrew would require one motor which adds weight to the propulsion system, but only required cables and wiring to transfer the energy as opposed to complex gearing and shafts. Depending on the type of battery and motors, additional components such as inverters and rectifiers would be needed to convert AC power to DC power and

vice versa. The cable weight, although not the majority of the propulsion system weight would also be included as well as weight for a power split unit to control each screws RPM independently.

7.2.1 Electric Power Technology

The weights of the electrical components, including the battery, will be sized according to the amount of power required for each one. The heaviest of these will be the battery which is sized for the most demanding segment of the mission and any efficiency losses through the powertrain. Sizing electrical components in the absence of detailed performance maps and size effects is done by calculating the required power of a component and dividing that by the components specific power. To implement this method, a technology assessment was performed to estimate properties of each component and ensure that the assumptions are reasonable for the time frame.

Battery: To benchmark the battery technology, car batteries (primarily Tesla) were used as current state of the art technology because they are certified and are of a similar scale. Their energy density is approximately 230-250 Wh/kg (356-387 Btu/lb) at the cell level which translate to approximately 190-210 Wh/kg (294-325 Btu/lb) at the pack level. Power density of these kinds of batteries is around 8-10 kW/kg (5-6 HP/lb) at the cell level and 6.5-8 kW/kg (4-5 HP/lb) when moving to the pack level. The efficiency varies slightly with manufacturer but is typically around 90-95%. Battery technology is growing at a steady pace, as seen in Figure 7.1 which shows batteries that either exist or are being developed as well as the overall trend [3]. Even a five year window can drastically affect the size of the electrical components. That being said, Table 7.1 below summarizes the technology assumptions used for sizing the batteries [4, 5].

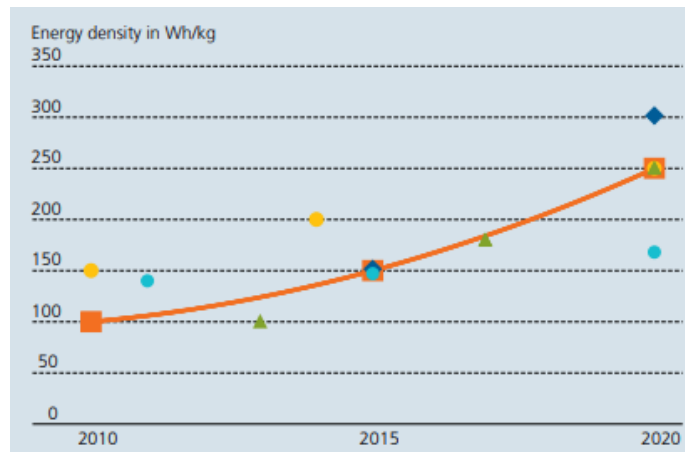


Figure 7.1 Battery energy density trend and prediction

Parameter	Value
Specific Power [kW/kg]	7 (4.3 HP/lb)
Specific Energy [Wh/kg]	200 (310 Btu/lb))
Efficiency [%]	93

Table 7.1 Battery technology assumptions

Electrical Components: There are other components in addition to the battery which also need to be sized using a similar approach. This includes the motors, inverters, rectifiers, cables and power split unit used in the electric powertrain. The motors were sized based on motor technology from the aviation industry, specifically from Siemens. The Siemens motor is a 261 kW (350 HP) motor with a specific power of 5.2 kW/kg (3 HP/lb) and an efficiency of 95%. The efficiency and specific power were kept constant while the rated power of the motor was allowed to change based on the sizing criteria. The inverters and rectifiers sizing assumed specific powers of 13.2 kW/kg (8 HP/lb) and efficiencies of 98%, while the power split unit sizing assumed a specific power of 200 kW/kg (122 HP/lb) and efficiency of 96%. In order to size the cables, the length of the cables needs to be estimated and a specific weight, rather than a specific power, assumed in terms of the weight per unit length (kg/m)(lb/ft). The assumed technology parameters are summarized in Table 7.2 below [6, 7, 8].

Component	Specific Power [kW/kg]	Efficiency [%]
Motor	5.2 (3 HP/lb)	95
Inverter/Rectifier	13.2 (8 HP/lb)	98
Power Split	200 (122 HP/lb)	96
Cables	1.5 (1 lb/ft)	98

Table 7.2 Electric Component technology assumptions

7.3 Propulsion Architecture Selection

The decision of which architecture to choose was not straightforward because it was largely dependent on the vehicle’s size and power requirements. Batteries are much less energy dense than fuel but are more efficient than an IC engine, so there is a breakeven point below which a battery architecture is lighter, and above which an IC engine architecture is lighter. The major factors in determining which powertrain to implement were complexity, flexibility, level of controllability, and estimated weight.

In terms of complexity, the electric option is slightly more favorable because components are connected to via cables which are essentially independent of component location whereas the mechanical option has less freedom because components need to be connect by shafts. This also corresponds to the flexibility of the two powertrains. The electrical components have much more flexibility

in terms of location compared to the engine and shafts which is a significant benefit when considering the weight and balance of the vehicle. Controllability is more difficult to quantify with models but assuming two sources of thrust (airscrews) a mechanical system is slightly worse. An electric system can make use of a power control unit to split power relatively easily while a mechanical system struggles to do this. It can be done to a degree but it imposes more constraints on the propulsion system such as having the engine be placed in between the thrust sources and having a shaft run out of each end. This allows for counter rotating shafts but also places limits on the angle of the shafts which in term affects the airframe and structure of the vehicle. Finally, in terms of estimated weight of each system the mechanical system is likely to be slightly lighter at first glance. As mentioned, fuel is much more energy dense which outweighs the lower efficiency of the engine but with the additional restrictions, more components like gears, shafts, and exhaust ducts will decrease the benefit in terms of weight reduction. Therefore, based on estimates of the payload (pilot), structure, and components, an electrically driven system was deemed to be the optimal architecture for this vehicle.

7.4 Human Power

Despite the necessity of modern power systems to sustain flight on *Il Mulinello*, human power was determined to be a key feature of Da Vinci's design, and thus its implementation on the vehicle was considered a priority. This section will discuss human power output capability and possible methods for human power augmentation.

7.4.1 Maximum human power output

As the team wished to include human power into the design of the vehicle to maintain Da Vinci's intention, an analysis of the maximum power output the pilot could produce was necessary. Moreover, it was also important to determine if the power output should be used directly (mechanical work), or converted into electrical work.

From the RFP, the mission requires an effort of at least one minute. For these estimations, done before a configuration was selected, a maximum flight duration of five minutes was considered, to allow for an error margin and a longer flight duration if the design permitted it.

The NASA Astronautics Data Book [9] presents the work capacity of a human, categorized as "champion athletes" and "healthy men". As expected, a person's peak rate depends on the effort length. The findings of the data book are presented in Table 7.3.

Filippone investigates the possibility of human powered flight in his article, Ref. [10]. He explains that the optimal power delivery is on a bicycle in a sitting position, and that the optimal pedaling speed is 90 - 110 RPM. This value is confirmed by Abbiss and al., Ref. [11]. This RPM value implies that, if the

Effort length (min)	Healthy man	Champion athlete
1	420 (0.56)	580 (0.78)
2	350 (0.47)	480 (0.64)
5	295 (0.40)	420 (0.56)

Table 7.3 Maximum work capacity in Watts (HP) from the NASA Data Book

work is to be used directly (mechanical work), reduction gears must be used to obtain the optimal rotor speed.

7.4.2 Mechanical to electrical power conversion and subsequent losses

The mechanical energy generated from pedaling can be converted to electrical energy. This is done using a generator or alternator. The electrical power can then be stored in a battery. According to Ref. [12], realistic generator voltage, current and power outputs for individual pedal generators are in the ranges of 12-40 V, 0-20 A, and 0-150 W (0-0.20 HP), with instantaneous peaks up to 750 W (1.00 HP). Losses in the conversion from mechanical to electrical power are small, since generators are 80-90% efficient [13]. If the current needs to be converted from DC to AC, an inverter must be used. Inverters' losses converting from 12 VDC to 110VAC are in the 85-95% range. The current can then be used directly, or be stored in a battery. A battery can have 10 to 35% losses [14], so using the current directly is beneficial if the power output has to be maximized.

It is clear that the maximum output possible for a five-minutes flight is around 400 W (0.54 HP), which is the initial value used to determine the output that can be expected for the mission.

If the power had to be converted to current, and assuming a 90% efficient generator, the power output from the generator would be 360 W (0.48 HP). Then, assuming a 95% efficiency in the inverter, the power output from the inverter would be 342 W (0.46 HP). If the current was used directly, one could assume a maximum power of 342 W, while if it was stored in a battery, the usage output power would be a maximum of 308 W (0.41 HP).

It is therefore recommended to use the mechanical work directly to minimize losses, and if this is not possible, then to minimize the conversions.

7.4.3 Pedal-assist systems

In order to alleviate the pilot's workload, a pedal-assist system was considered. Today's expanding electric bike market offers a variety of options that could be used to contribute to powering the front propeller, complementing the pilot's own pedaling. Different systems used today were analyzed to determine if adding such pedal-assist to the airscrew was beneficial without adding too many constraints, and if so, which system was to be used. There are two main categories of eBike motors: mid-drive motors and hub-drive motors.

The hub-drive motors are located in the middle of one wheel (usually the rear wheel). It drives the wheel directly. In a traditional bike, the offset location of the motor can create a weight imbalance in the bike, and cause steering difficulties for the driver. These problems are specific to regular bikes, but will not affect an airscrew propeller.

The mid-drive motor is located between the pedals, supplementing the pedaling power within the bike’s chain-drive. This position allows for the mid-drive motor to work “synergistically” with the bike’s gear, giving the motor a higher efficiency than the hub-drive in regular bikes. Indeed, the hub-drive location causes it to spin slower than the mid-drive. The mid-drive, when the rider pedals at a normal rate (50-100 RPM), turns at an efficient RPM. Once again, this problem might not affect an aerial screw. Indeed, the propeller RPM will be higher than the normal pedaling rate (around 600 RPM), and closer to an efficient RPM.

While the advantages and disadvantages of mid- and hub-drives are specific to bikes, and do not affect the aerial screw, the mid-drive systems are more advanced than the hub-drive systems. Therefore, if a system were to be used in this project, it would be a mid-drive system.

All the state-of-the-art pedal-assist systems have comparable efficiencies and weights. For brevity, only one mid-drive system was used to determine expected characteristics for this vehicle’s system: the Shimano STEPS E8000. The Shimano STEPS E8000 (Fig. 7.2) is often ranked amongst the top three e-Bike systems in the market. The components characteristics of the system relevant to our application are presented in Table 7.4. The pedal assist in this application would only need a drive unit, a battery, and a speed sensor. These three components add a weight of less than 6 kg (13 lb) to the vehicle.

Component	Model	Weight, kg (lb)
Drive unit	DU-E8000	2.88 (6.35)
Drive unit cover	SM-DUE-80-A/SM-DUE-80-B	
Battery	BT-E8010	2.6 (5.73)
Battery mount	BM-E8010	
Speed sensor	SM-DUE10	0.060 (0.13)

Table 7.4 Shimano STEPS E8000 components information

After exploring the idea of using pedal assist, the team determined that it would be beneficial to increase the speed and range of the vehicle. Indeed, with pedal assist, the pilot could stop pedaling without compromising the range of the mission. The mission does not require a minimum speed, and the range is small enough to allow for the pilot to pedal at a comfortable rate without tiring. Therefore, the team decided not to include a pedal-assist unit to *Il Mulinello*. If the demonstrator is successful, however, pedal assist could be added to the design to create a more accessible personal vehicle.

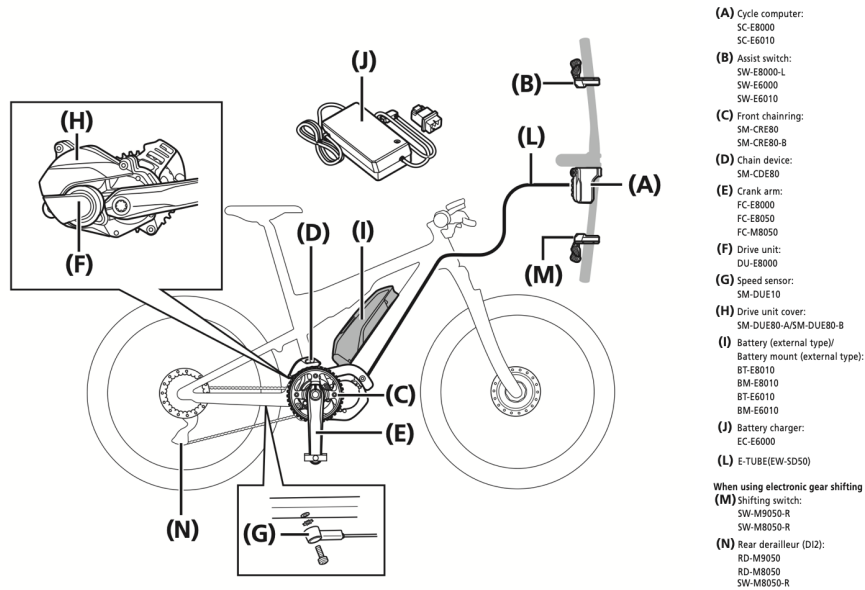


Figure 7.2 Shimano STEPS E8000 system on a bike (from Shimano’s user manual)

8 Controls and Piloting

Using airscrews for the main rotors presented a particular problem for controllability of the aircraft. Conventional rotorcraft primarily use variable blade pitch to control the pitch, roll, and yaw of the vehicle. Attempting to mimic this with an airscrew-style rotor was impractical for several reasons. First, control laws do not exist for such a control system, and there is not enough aerodynamic data on airscrew rotors to generate them from scratch. Secondly, there was the challenge of finding a material which is both flexible enough to allow for high levels of controllability and stability of the vehicle while also being strong enough to withstand the aerodynamic loads required for a main rotor. Finally, manufacturability was already a concern for a main rotor with such complex geometry without including deformable structures and advanced materials. As such, an alternative control system was necessary.

The aircraft is controlled by two primary control systems. First, the forward propeller is capable of changing direction from left to right, giving the pilot direct control over the yaw of the vehicle. This system is detailed in figure 8.1(a) with deflection simulated in figure 8.1(b). Combined with the fact that the forward propeller is powered by the pedaling system, the pilot is given direct

control over two degrees of freedom present in a conventional ground vehicle, namely throttle and yaw. Roll and pitch are controlled by an autopilot using external flaps in the wake of the main rotors with the goal of maintaining stable level flight. There are also a couple of secondary effects which give the vehicle additional stability. First, the vehicle has natural stability due to the angular momentum of the main rotors. Similarly to a bicycle, the inertia of the main rotors will resist deflection of the axis of rotation, providing a restoring moment in response to roll and pitch motion. Secondly, the pilot is able to shift his or her weight, and when paired with yaw control inputs, again, analogous to a bicycle. This provides natural roll stability. The control system responsible for driving the automated flaps is described in detail in section 9.

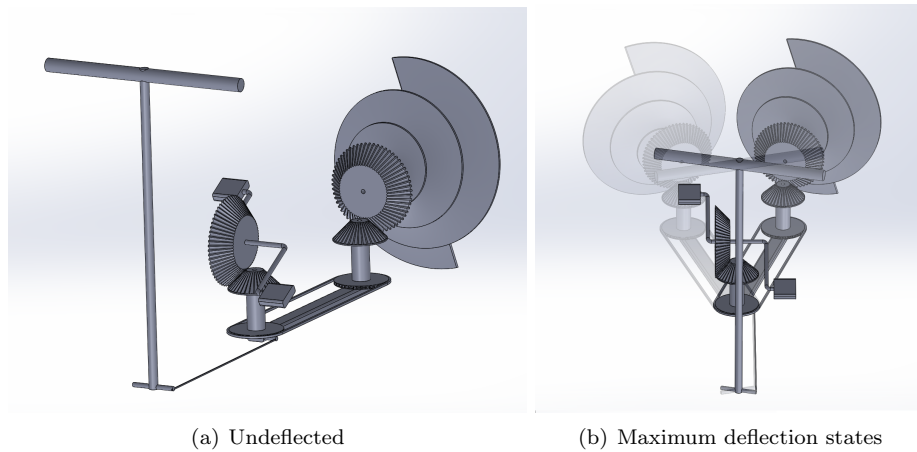


Figure 8.1 Propeller control system

9 Flight Control System Concept

As explained in section section 8, the vehicle could not use the control system from a conventional rotorcraft. Conventional helicopters use collective, cyclic and anti-torque controls. In this design, the anti-torque is not needed, as the tandem airscrew removes the need for this. Collective and cyclic controls would require a modification on the airscrew, and as stated previously, this is not feasible. Therefore, the team had to design an alternate control system.

The dependence on the dual airscrews to maintain torque balance, and the impossibility to add a swash plate to the airscrews led to the addition of a front propeller. The front propeller controls the forward motion and the yaw control.

To control roll and pitch, four external flaps controlled by autopilot were introduced.

9.1 Equations of Motion

The equations of motion for the vehicle are described in equations 10, 11 12, 13, 14, and 15, where the symbols are outlined in Table 9.1. Here it is assumed that vehicle drag is negligible, all flaps have the same area and are located the same distance from the center of gravity of the vehicle, the flaps are on the same vertical plane as the center of gravity of the vehicle, the flaps obey thin airfoil theory, the rotor downwash is purely vertical, and both rotors produce the same thrust and torque.

$$F_p \cos \gamma = m \ddot{x} \quad (10)$$

$$\pi \rho w^2 S (\delta_1 - \delta_2 + \delta_3 - \delta_4) + F_p \sin \gamma = m \ddot{y} \quad (11)$$

$$\frac{1}{2} \rho w^2 S (C_D(\delta_1) - C_D(\delta_2) + C_D(\delta_3) - C_D(\delta_4)) + 2T - W = m \ddot{z} \quad (12)$$

$$\frac{1}{2} \rho w^2 S y_f (C_D(\delta_1) - C_D(\delta_2) + C_D(\delta_3) - C_D(\delta_4)) + M_p \cos \gamma = I_x \ddot{\psi} \quad (13)$$

$$\frac{1}{2} \rho w^2 S x_f (-C_D(\delta_1) - C_D(\delta_2) + C_D(\delta_3) + C_D(\delta_4)) = I_y \ddot{\phi} \quad (14)$$

$$\pi \rho w^2 S x_f (-\delta_1 + \delta_2 - \delta_3 + \delta_4) + F_p \sin \gamma L_p + M_p \sin \gamma = I_z \ddot{\theta} \quad (15)$$

m	vehicle mass	T	rotor thrust
I_x, I_y, I_z	moments of inertia	$\ddot{\psi}, \ddot{\phi}, \ddot{\theta}$	angular accelerations
M_p	propeller torque	γ	Propeller deflection angle
ρ	density of air	w	main rotor downwash
δ_i	deflection angle of flap i	C_D	flap drag profile
$\ddot{x}, \ddot{y}, \ddot{z}$	components of acceleration	F_p	propeller thrust
L_p	prop rotation center	S	flap planform area
x_f, y_f	flap location coordinates		

Table 9.1 Table of variables for equations of motions

9.2 Yaw Control and Throttle

The vehicle design was inspired by recumbent bicycles, with the pilot laid-back in a reclined position. Following that idea, it was decided to allow the pilot to control the yaw directly, using a bicycle-like handlebar. This system is illustrated in Figures 8.1(a) and 8.1(b).

The front propeller, in addition to yaw control, provides forward thrust. Using the aerodynamic study detailed in section 6.1 and the size of the front propeller, it was determined that the pilot could provide enough power to run

the propeller at 600 RPM. The optimal human pedaling speed, as explained in subsection 7.4, is 100 RPM. A gear reduction system was therefore designed to allow for an optimum RPM for both the pilot and the propeller, with a 1:6 gear ratio.

9.3 Roll and Pitch Control

Using the equations of motion detailed earlier, a state-space model was developed for the system. A control system used to control the roll and pitch motion of the vehicle was developed using model predictive control, following the methodology outlined by Theodorou [15]. This code is detailed below. As the front propeller deflection angle and rotational speed is controlled by the pilot, and not by the system, the model assumes a constant value for the propeller deflection angle γ and the propeller thrust F_p .

The code employs an iterative process to determine the optimal gain to be used to return to equilibrium in case of a disturbance, by predicting the trajectory, or a way to achieve the goal, and calculating its error, as summarized in Figure 9.1. In this case, the goal is to return to equilibrium. The inputs are the initial state of the system, and the desired goal state. The state matrix A and input matrix B are used, along with an avoidance matrix Q and a sensitivity matrix R which determine the weights associated with the control. The Q matrix penalizes the error on each state by increasing the cost function using the weights assigned to each state variable. These weights can be all equal, but for a more efficient control system, different weights for each variables are desirable. Each variable was assigned a certain importance, depending on the impact a high error on that variable would have. For example, an error in the x direction was assigned very little weight, as the vehicle doesn't need to be extremely stable in that direction. On the other hand, an error in the roll is heavily penalized, as it would cause an undesirable position for the vehicle.

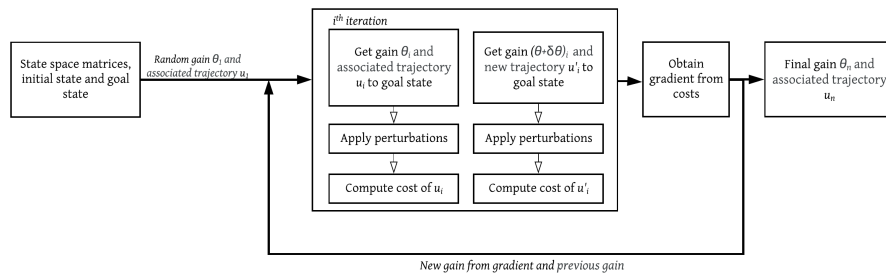


Figure 9.1 Diagram of the iterative control system for n iterations

Initially, a random trajectory and a random gain are generated. In each iteration, the current trajectory is "disturbed" with a random input, and the cost (defined as the distance between the current state and the goal state) associated with the disturbed trajectory is calculated. The gain is then increased

by an infinitesimal amount, and used to obtain a new trajectory. Like the first trajectory, this one is also disturbed, and the cost associated with it is calculated. These two trajectories, obtained with the current gain and its slight variation, are used to determine the gradient vector. The current gain is then multiplied by the gradient and the learning rate, and become the gain used in the next iteration. This process is repeated for a finite number of iterations. The feedback control policy is used to stabilize the system while minimizing cost.

As shown in Figure 9.2, the cost decreases with each iteration, and converges to a minimum of less than one. The figure shows three different runs. Since every run involves multiple random disturbances to the system, it is notable that each run is distinct from one another. However, the difference between each run is negligible and therefore the analysis of the effect of each input on the controls can be made using any arbitrary run.

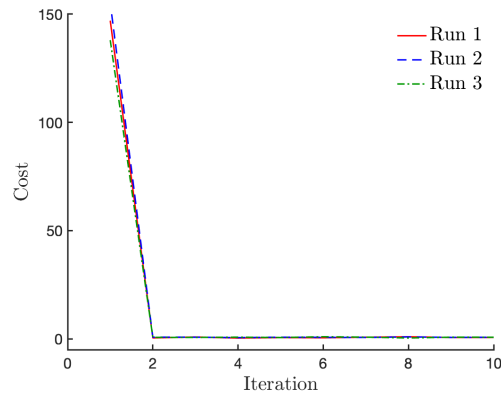


Figure 9.2 Cost of the calculated trajectory at each iteration for three different runs

The behavior of the cost and its convergence rate depends on multiple factors. The learning rate, used to determine the improved gain for each following iteration, affects the cost convergence rate. As the learning rate decreases, the cost converges faster (as soon as the second iteration), as shown in Figure 9.3.

10 Component Layout

With the constraints placed on the vehicle, a goal of the component placement was to minimize the footprint of the vehicle and decrease wasted space. This meant making things as compact as possible while still being able to achieve the mission requirements and having the vehicle be controllable by the pilot. A secondary goal of the component placement was to help keep the vehicle stable and balanced and so the components are all placed on the $x - z$ plane such that

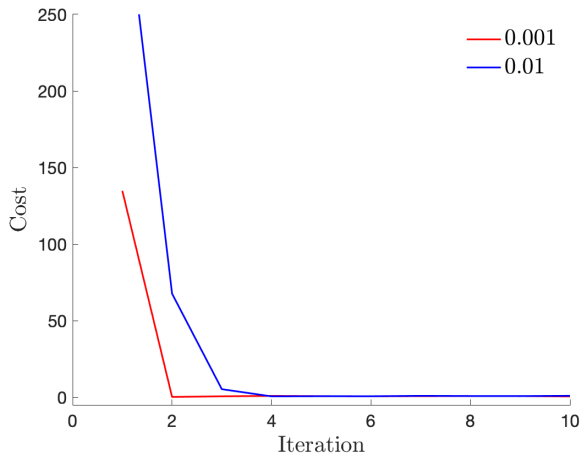


Figure 9.3 Cost of the calculated trajectory at each iteration for different learning rates

their centers of gravity have a y location of zero. To further aid the roll stability, the center of gravity was chosen to be lower to the ground and away from the lift generated by the airscrews so most components are placed at or below that pilot's center of gravity. To ensure pitch stability, the weight also needed to be distributed equally in the forward and aft sections of the vehicle.

Other than the pilot, the batteries are the heaviest component of the vehicle and thus are placed behind and below the pilots seat. The aircrews are relatively fixed in that they cannot be placed any lower for the safety and visibility of the pilot. The motors are connected to the aircraft shafts and thus lie on a vertical line through the aircrews but are placed near along the x -axis of the vehicle. The airscrews, motors, battery, powersplit unit, and control surfaces are all sized during each iteration of the vehicle sizing so their locations and weights are updated accordingly but stay in the same general locations.

11 Structures and Materials

Structural design for *Il Mulinello* involved taking inspiration not only from modern advances in vertical flight but also from the elements that inspired Da Vinci's original design. It is easy to get carried away with materials and manufacturing processes that would seem alien to the Renaissance engineers of Da Vinci's time. Keeping true to the spirit of Da Vinci's original concept allows for a design that both showcases the modern innovations of engineering and celebrates the imagination of the past.

11.1 Airframe Material

When choosing a material for any aircraft, great care must be taken to strike a balance between weight, strength, manufacturability and cost. For the design of this airframe, the main material studied for usage was aluminum. Aluminum has a vast historical usage in aircraft and provides great strength to weight characteristics that have made a popular choice for use since the dawn of flight. In addition to its beneficial material properties, aluminum is very readily available at low cost while also boasting great levels of machinability. Many alloys of aluminum exist with varying properties that make them suitable to various applications. One of the most commonly used alloys of aluminum is 6061. This is a hardened aluminum alloy containing magnesium and silicon as its major alloying elements and is used heavily in the aerospace industry for structural applications. In particular, the T6 temper often applied to aluminum 6061 will result in a yield strength of around 240 to 270 MPa (34810 - 39160 psi). The wide use of 6061-T6 also provides a wide variety of extrusion types and sizes that allows for flexibility in the airframe design.

11.2 Airframe Design

Da Vinci's original concept envisioned a contraption that could utilize human power to achieve vertical flight. This original interpretation inspired many of *Il Mulinello's* design choices in order to stay true to Da Vinci's original vision. The primary desire of the airframe design was to take an everyday human powered vehicle and transform it into something that can achieve flight. Naturally, this inclination led to a re-imagining of a bicycle. More specifically, *Il Mulinello's* design revolved around a more aerodynamic version of a traditional bicycle: the recumbent bicycle. Not only does the low down seating position help provide optimum weight balance characteristics for the vehicle, allowing the airscrews to be positioned lower and reducing the overall height of the frame, but also allows for the turning system to be much more compact and provide an additional level of safety for the occupant as the distance between their head and the blades is greatly increased.

11.3 Airscrew Material

Material selection for rotorcraft blades is an ever-growing field that often pushes the boundaries of structural design. Blades must be able to withstand high levels of dynamic loading and large bending moments. The materials chosen must be flexible in order to minimize stress in the material yet care must also be taken to minimize deflections in the material to maintain the integrity of the of the aerodynamics. Weight also becomes a crucial factor to reduce power requirements as much as possible.

Two primary classes of materials were looked at as suitable candidates for the airscrew blade design. The first of these are thermoplastics. Thermoplastics are polymers that are highly pliable at elevated temperatures and solidify upon

cooling. This property of the material lends itself to a high level of versatility when it comes to manufacturing complex shapes. Types of thermoplastics include ABS, acrylic, nylon and PLA. The second category of materials studied were reinforced plastics. These typically combine epoxies, resins, or thermosetting plastics with fibers to create strong composite materials. Materials such as carbon fiber have a storied history being utilized to make lightweight aerodynamic components for automotive and aerospace applications, making them an enticing prospect for the airscrew. However, the complexity in manufacturing complex shapes, especially a helical one such as the airscrew, means its feasibility comes into question. Metals were not looked due to the relatively low loading on the airscrew and a need to keep weight to a minimum. From the Pugh matrix of materials, shown in Table 11.1, the chosen material for the airscrew was nylon as it is able to withstand the loads while minimizing cost and complexity.

Criteria	Weight	ABS	Nylon	PLA	Carbon Fiber
Specific Strength	0.3	1	2	1	4
Machinability	0.1	4	2	2	1
Manufacturability	0.2	3	3	3	1
Stiffness	0.2	1	4	2	2
Durability	0.1	2	3	2	4
Aesthetics	0.1	2	3	2	1
Totals	1	1.9	2.8	1.9	2.4

Table 11.1 Weighted Pugh matrix comparing possible airscrew material choices

12 Rotor and Airframe Loads

Determining the loads an aircraft is subject to is a vital first step into validating the structural design of a concept. To develop a range of static loading parameters, the weight estimate of the vehicle is first determined. From there typically an upper bound for acceleration limits are established based upon mission parameters. In the case of *Il Mulinello*, there are no requirements for acceleration or velocity so the control system can be designed such that take off and landing are performed in a gentle fashion to minimize any excessive loading parameters. Historically, however, many aircraft designs tend to fall out of design parameters and assumptions (often by, quite literally, falling) and therefore the estimated maximum static load was multiplied by a factor of safety of 1.5 to ensure the vehicle operates well below structural limits. This static loading was then split evenly amongst the two airscrews, giving a final loading on each airscrew a value of 2000 N (450 lb). In addition, a centrifugal force must be applied to each of the airscrews. This force can be derived from an estimated mass and the operating rotational velocity of each airscrew. For dynamic loading of the airscrew, the use of a symmetric airscrew design minimizes vibratory loading at hover

which will be assumed to hold true at forward flight given the low velocity of the aircraft.

13 Structural Analysis

To properly assess the structural capabilities of the airscrew and airframe design, finite element analysis utilizing SolidWorks was done. The airframe was analyzed by inputting the static loads described in the previous section at each of the airscrew mounting points. The airscrew was also analyzed using static loading. However, the airscrew loading had to be approached in a manner consistent with the understanding of the aerodynamic effects at play. From the CFD analysis, it is known that the vast majority of the lift is produced by a small section of the blade just after the leading edge. In addition, the forces must also taper down to zero as they move towards the root of the blade in order to mimic the loading seen by the airscrew in the real world. With this in mind, half the total maximum static load was applied to the upper surface of the airscrew such that the forces linearly tapered down to zero with decreasing height and tapered down to zero with decreasing radius.

To undergo the FEA, the best material from the initial analysis in section 11.3 was chosen (Nylon 6/10). The results of the first pass of the FEA saw deficiencies in the rotor shaft design as the highest bending moments were concentrated here. To increase the load capacity of the shaft, the shaft material was chosen to be aluminum with a 0.05 m (2 in) diameter and 0.00635 m (0.25 in) thickness. The analysis saw a maximum von Mises stress of 47 MPa (6820 psi), well below the maximum tensile strength of 86 MPa (12470 psi). In addition, the minimum safety factor of the screw was found to be 1.34, located at the bottom of the shaft. However, the maximum deflection of the rotor was relatively high (0.022 m or 0.87 in). To mitigate this, the actual rotor design will incorporate aluminum spars bonded at the leading edge of the rotor, taking inspiration from the design of the test rig from section 5.2.

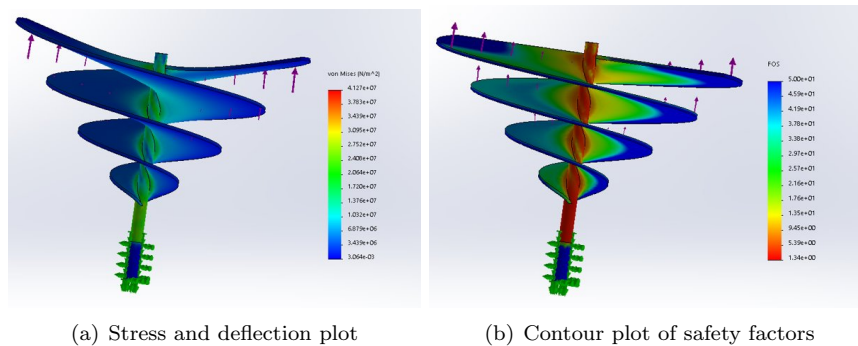


Figure 13.1 Airscrew FEA analysis results

14 Concept Validation

With all subsystems now defined and analyzed and because of the unique nature of the requirements and chosen configuration, concept validation is required to ensure the design is realizable. For this, a list of fundamental capabilities was formed and *Il Mulinello* was analyzed against this list to make sure that all capabilities are accounted for in the design. These capabilities come from standard rotorcraft requirements, an interpretation of the RFP requirements, and requirements unique to the chosen design. This section will describe how each capability is fulfilled by the proposed design and analysis thereof. These capabilities are as follows:

1. Greater lift generation capability than required weight via airscrew rotors
2. Pilot control of vehicle velocity, attitude, and altitude
3. Vertical take-off and landing
4. Stable hover and forward flight
5. Pilot power generation
6. Structural integrity
7. Vibratory load mitigation and damping
8. Power splitting and transfer
9. Power storage

Capability 1 is fulfilled through the iterative component sizing process described in section 3. This process takes an initial guess at the gross weight of the vehicle, sizes the components appropriately to generate the required lift, computes a new gross weight, and iterates until the gross weight no longer changes. By design, this ensures that the weight of the vehicle does not exceed its lifting capability. Capability 2 is fulfilled through three mechanisms. First, a throttling system for the main rotors gives the pilot altitude control by varying the RPM of the main rotors and thus the total thrust produced. Second, the pilot's pedaling system gives the pilot control of *Il Mulinello*'s forward velocity by varying the RPM of the forward propeller. Finally, the turning system gives the pilot attitude control by determining the angle of the forward propeller's thrust vector. Capability 3 is fulfilled through the tandem rotor design, where in the absence of pilot pedaling, thrust is purely vertical. Stability during takeoff and landing is ensured by the autopilot controls of the flaps in the wakes of the main rotors. Capability 4 is fulfilled through the stability analysis the design of the robust control system described in section 9. Capability 5 is fulfilled by the pedaling system by which the forward propeller is powered. This allows for human powered flight without relying on human power to keep the vehicle airborne. Capability 6 is fulfilled through the structural analysis and robust airframe design presented in section 13. Capability 7 is fulfilled by assuring that

the weight and lift distribution of the rotors is balanced around the shaft, that the structural integrity has a moderate factor of safety, and by ensuring that the pilot is isolated from vibrations. Capability 8 is fulfilled through the design of the electrical system described in section 7 which transfers power from the batteries to a power split unit and then to the motors. With these capabilities accounted for and the responsible systems thoroughly analyzed, confidence in the final designs ability to meet the requirements set out in the RFP is assured.

15 Capability, Performance and Requirement Compliance

The minimum requirements laid out by the RFP were that the majority of lift and thrust was generated by airscrews, defined as a single-bladed rotor with solidity at least 1. *Il Mulinello* generates lift using a tandem configuration of two pairs of coaxial airscrews which conform to the definition in the RFP. Thrust is generated with a forward facing coaxial airscrew which is a scaled version of the main rotors, and thus also conforms to the RFP requirements. The minimum mission set out by the RFP was as follows:

1. Vertical takeoff to 1 m altitude
2. Hover for 5 seconds at 1 m altitude
3. Forward flight over 20 m for at least 1 minute at 1 m altitude
4. Hover for 5 seconds at 1 m altitude
5. Vertical landing from 1 m altitude

This mission sets the minimum endurance of the vehicle at 1 minute 10 seconds with additional time for takeoff and landing. At 101% hover power, *Il Mulinello* will reach 1 m altitude in roughly 4 seconds (equation 16), and assuming a similar time for landing, the total minimum endurance is roughly 1 minute 18 seconds. The batteries were sized to meet the more restrictive of the power and energy requirements for the vehicle. Since the power requirement was determined to be more restrictive, the batteries are capable of generating 8727 Watt-hours (29800 Btu) of energy (equation 17), while the energy requirement to perform the minimum mission is only 2954 Watt-hours (10000 Btu) (equation 18). As such, the vehicle is able to exceed the minimum endurance requirements by nearly 300%. This calculation assumes that the rotors are performing at hover efficiency during the forward flight phase. Assuming the vehicle flies at the lowest possible speed in order to maximize the rotor efficiency while meeting the range requirement, this gives a forward flight velocity of 0.1 meters per second (0.3 ft/s) for an advance ratio of 0.0004, well within the range where forward flight effects will be negligible. This inspires confidence that there is room for an increase in flight velocity and thus an increase in the range capability of the

vehicle. Assuming that forward flight effects are negligible up to an advance ratio of 0.01, the vehicle range could be as much as 500 m (1640 ft) (equation 19). To further validate this number, it is necessary to ensure that this advance ratio is achievable with human power. Using CFD data for the figure of merit of the dual airscrew design and the power output capability of a human pilot, one can estimate what the drag coefficient of the full vehicle would need to be to prevent forward flight at an advance ratio of 0.01. This drag coefficient was determined to be roughly 1.3 (equation 20), which is in the range of drag coefficients for bluff bodies. A worst-case value for the drag coefficient may be around 2.1, similar to a rectangular box, where the range of the vehicle would still achieve a value of nearly 400 meters (1300 ft) (equation 21), far exceeding the minimum range requirement described in the RFP. A table of variables for equations 16-21 can be found in table 15.1. While *Il Mulinello* far exceeds the range and endurance requirements of the RFP, since power is the limiting factor in the vehicle design, the capability of *Il Mulinello* to reach higher altitudes is bounded. The airscrews suffer the same loss of rotor efficiency with increasing altitude as a conventional rotor, and so when atmospheric conditions begin to deviate significantly from those at sea-level, *Il Mulinello* will struggle produce the lift necessary to maintain level flight. However, these altitudes should still far exceed the minimum requirement of 1 meter set in the RFP.

$$t_t = \sqrt{\frac{2h}{P_r^{1.5}g}} \quad (16)$$

$$E = \frac{P}{p_b} e_b \quad (17)$$

$$E_r = Pt \quad (18)$$

$$R = Ut \quad (19)$$

$$C_D = \frac{(P_h \mu \sqrt{2\rho A})^{\frac{2}{3}}}{0.5\rho U^2 S} \quad (20)$$

$$R = \sqrt{\frac{(P_h \mu \sqrt{2\rho A})^{\frac{2}{3}}}{0.5\rho C_D S}} t \quad (21)$$

16 Maneuverability and Workload

As explained in previous sections, the team wanted to maintain Da Vinci's vision when designing the vehicle, which is why it was decided to incorporate a pedal system. This meant that *Il Mulinello* had to evoke a bicycle, but also that the pilot couldn't be overwhelmed with tasks other than pedaling. It was therefore

h	take-off height	P_r	take-off power ratio
g	gravitational acceleration	P	vehicle power requirement
p_b	battery specific power	e_b	battery specific energy
E_r	Energy Requirement	t	flight time
R	Range	U	forward flight speed
C_D	vehicle drag coefficient	P_h	human power capability
μ	figure of merit	ρ	density of air
A	propeller disk area	S	Vehicle Area Reference

Table 15.1 Table of variables for performance calculations

decided that the pilot should have the same workload a cyclist has: piloting and simple directional control.

To obtain an optimal pedaling power usage, the pilot should pedal at 100 RPM. While this cadence demands a higher power output from the pilot, it is sustainable in short time intervals, like it is the case in this mission. Moreover, as the pedaling only controls the forward motion of the vehicle, the pilot may stop and rest if desired, or pedal at a lower cadence when tired. Like a cyclist, the pilot must hold the handlebar while pedaling and control the yaw of the vehicle. Moreover, the pilot might choose to shift his or her weight to provide additional roll stability.

Overall, the pilot of the aircraft will not be overwhelmed, as the workload is similar to that of a cyclist riding a bike.

17 Accommodation, Accessibility, Human Factors

The most basic requirement of the vehicle was the ability to support a human payload, and this factor formed the basis for nearly every design decision. It was ensured that there was sufficient space for a human pilot to occupy, and the pilot interface components, such as the seat, handlebars, and pedals, needed to be sized and placed with pilot comfort in mind. First, a pilot posture needed to be decided on. The factors influencing this decision were the presence of the rotors above the pilot, the space needed for the forward propeller turning system, and the placement of power system components. A reclined posture allows the rotors to be lower, resulting in a shorter shaft length and lower shaft bearing moments. It also allows the rotors to be spaced further apart so that there are fewer losses in efficiency due to rotor-rotor interference. Finally, it allows the pilot weight to be distributed on a relatively stable axis of the vehicle for a favorable impact on the vehicle moments of inertia. Once this posture was chosen, the handlebars and pedals could be appropriately placed based on median human proportions. The diameter of the pedals was chosen to match those on bicycle systems assuming that the appropriate optimization has already been done in that field. Since the pilot's head is directly in the wake of the rear

rotor, the pilot must wear a helmet when the rotors are powered up. In addition, the pilot restraint harness will act a safety ‘kill-switch’ of sorts, allowing the rotors to only be powered when the harness is locked and secured, reducing the chance of injury during ingress and egress of the vehicle.

18 Demonstrating Manufacturing and Feasibility

Fostering a greater understanding for the aerodynamics of the aerial screw encapsulates the ultimate objective of this design study. While the great advances in engineering and analysis made over the centuries since Da Vinci’s time have been taken advantage of here, the secondary objective of the study was to also remain true to the spirit of the original vehicle and be of a design that Da Vinci would be able to understand had he been alive today. This overarching goal was embodied in every aspect of the vehicle design and resulted in an unexpected benefit; the feasibility of the vehicle is quite high. The vehicle does not rely upon technology or manufacturing methods that are beyond current capabilities and many of the assumptions made are fairly grounded in reality. The electrical system operates on the higher end of typical motor efficiencies but still fall within reasonable bounds. The final step towards determining the feasibility of the project would be to undergo the small-scale experiment proposed in section 5.2 to validate the performance characteristics developed for the airscrew.

All of the proposed design elements in this paper utilize common manufacturing methods that are employed daily and require little to no tooling. The frame made of simple aluminum tubing can be bent and welded together while the airscrews themselves can be extruded and both bonded and mechanically attached to aluminum shafts. The gearbox for the turning system mimics conventional systems found in many vehicles today and would require fairly little complex machining. All these factors combine to create a robust yet simple vehicle able to embody the spirit Da Vinci instilled into his first concept for the aerial screw and all the rotorcraft that subsequently followed.

19 Project Summary

The goal of this endeavor was to gain insight into the aerodynamics of Leonardo Da Vinci’s Aerial Screw and its feasibility in a vehicle design. To better understand the physics behind the concept and the parameters of interest, computation fluid dynamics analysis was performed on several screw configurations to determine which one provided the best performance. With Leonardo’s vision in mind, several vehicle configurations were considered and a tandem rotor design, modeled after a bicycle, was chosen. The reasons behind this are three fold, to ensure stability of the vehicle, to reduce the power requirements, and to stay true to what Leonardo may have designed if he were alive today. Using this analysis to guide the vehicle design, a propulsion architecture was then chosen to min-

imize losses and provide the required power to sustain flight and complete the mission. The vehicle structure was then created to again minimize weight while ensuring structural soundness with built in safety factors. This included determining materials appropriate for each component with manufacturing, cost, and function in mind. Finally, as the vehicle also needs to be controllable, a control system was designed to allow the pilot to steer the vehicle and the vehicle was then sized to the design mission.

In addition to the mission requirements, the team felt that aesthetics and resemblance to Da Vinci's original design were important factors to incorporate into the vehicle's design. This led to the vehicle being at least partially human powered as was originally intended. The final design features two airscrews which supply the lift required to maintain hover as well as a forward facing airscrew which is powered and steered by the pilot for forward flight and turning. The power supplied to the airscrews is delivered by two electric motors which are connected to a powersplit unit and powered by a lithium-ion battery. This avoids clunky engines and emissions and is quieter than the mechanical alternative. The structure is streamlined and made of light materials to improve vehicle efficiency, and control flaps are located in the forward and aft sections of the vehicle to provide the necessary controls to complete the mission safely. The final vehicle has the capability to go beyond the minimum required mission with current state of the art technology assumptions and weighs about one third the weight of a smart car.

References

- [1] Johnson, W., *Helicopter Theory*, Princeton University Press, 1980.
- [2] Leishman, J. G., *Helicopter aerodynamics*, Cambridge University Press, 2000.
- [3] Thielmann, A., Sauer, A., Isenmann, R., and Wietschel, M., “Technology Roadmap Energy storage for Electric mobility 2030,” 2012.
- [4] Bower, G., “Tesla Model 3 2170 Energy Density Compared To Bolt, Model S P100D,” 2019.
- [5] Holland, M., “The Ultracapacitors, Electrodes, and Battery Manufacturing Tech Tesla Gets With Maxwell Technologies,” 2019.
- [6] Dyson, R., “NASA Hybrid Electric Aircraft Propulsion,” Presentation, 2017.
- [7] Armstrong, M., “Architecture, Voltage, and Components for a Turboelectric Distributed Propulsion Electric Grid,” *NASA Technical Reports Server*, 2015.
- [8] Tacke, W. and Boric, M., “World Directory of Light Aviation 2015-16,” *World Directory of Light Aviation*, 2015, pp. 262–263.
- [9] Parker, J. F. and West, V. R., “NASA Bioastronautics Data Book,” *Bioastronautics Data Book*, 2nd ed., 1973, pp. 866–870.
- [10] Filippone, A., “On the Possibility of Human-Powered Vertical Flight,” *Journal of the American Helicopter Society*, Vol. 52, No. 4, 2007, pp. 371.
- [11] Abbiss, C., Peiffer, J., and Laursen, P., “Optimal Cadence Selection During Cycling,” *International SportMed Journal*, Vol. 10, No. 1, 2009.
- [12] Gilmore, A. M., “Human Power: Energy Recovery from Recreational Activity,” *Guelph Engineering Journal*, Vol. 8, No. 16, 2008.
- [13] Spooner, E. and Chalmers, B. J., “TORUS: A slotless, toroidal-stator, permanent-magnet generator,” *IEE Proceedings-B*, Vol. 139, No. 6, Nov. 1996.
- [14] Stevens, J. and Corey, G., “A study of lead-acid battery efficiency near top-of-charge and the impact on PV system design,” *Conference Record of the Twenty Fifth IEEE Photovoltaic Specialists Conference - 1996*, IEEE, Washington, DC, USA, 1996, pp. 1485–1488.
- [15] Theodorou, E., *Machine Learning for Control Systems*, Evangelos A. Theodorou, 2015.